Research Square

Preprints are preliminary reports that have not undergone peer review.
They should not be considered conclusive, used to inform clinical practice,
or referenced by the media as validated information.

Differential lipid selectivity of StARD phospholipid transporters revealed by native MS

Carol Robinson

carol.robinson@chem.ox.ac.uk

University of Oxford https://orcid.org/0000-0001-7829-5505

Carla Kirschbaum

University of Oxford https://orcid.org/0000-0003-3192-0785

Sophie Lawrence

Kavli Institute for Nanoscience Discovery https://orcid.org/0009-0005-6652-4792

Jack Bennett

University of Oxford

Olivia Ramsay

Kavli Institute for Nanoscience Discovery

Yara Ahmed

University of Fribourg

Tarick El-Baba

University of Oxford https://orcid.org/0000-0003-4497-9938

Stefano Vanni

University of Fribourg https://orcid.org/0000-0003-2146-1140

Article

Keywords:

Posted Date: January 21st, 2026

DOI: https://doi.org/10.21203/rs.3.rs-8591680/v1

License: This work is licensed under a Creative Commons Attribution 4.0 International License.
Read Full License

Additional Declarations: There is **NO** Competing Interest.

Version of Record: A version of this preprint was published at Nature Communications on August 22nd, 2026. See the published version at https://doi.org/10.1038/s41467-026-76988-1.

Abstract

Intracellular lipid transport in eukaryotes is largely mediated by lipid transfer proteins (LTPs). Transport kinetics differ markedly among lipid species, implying selective lipid recognition by the involved proteins. Here, we characterize endogenous ligands of the human phospholipid transporters STARD2, STARD7 and STARD10 by multistage native mass spectrometry (MS). Our results demonstrate that they exhibit distinct lipid selectivities, with STARD7 binding a broad range of phospholipids, whereas STARD2 and STARD10 preferentially copurify with poly- and di-unsaturated phospholipids, respectively. We link this acyl chain selectivity to tissue-specific LTP expression patterns and show that LTP expression levels modulate lipid biosynthesis. Through site-directed mutagenesis and molecular dynamics simulations, we further identify a conserved arginine that is essential for phospholipid binding in STARD7 but dispensable in STARD2 and STARD10. To investigate regulation of LTP activity, we mapped phosphorylation sites by native top-down MS and found that STARD2 and STARD10 are phosphorylated in membrane-binding regions. Liposome-based assays revealed that phosphorylation abolishes lipid transfer activity of STARD10 and that lipid selectivity influences the transfer rates of different lipid probes. Together, our results demonstrate that LTPs exhibit distinct lipid binding preferences and suggest that cells finely tune lipid homeostasis through regulating LTP expression levels and activity.

Introduction

Eukaryotic membranes are defined by unique lipid compositions tailored to support organelle-specific functions.[1] To maintain distinct lipid profiles across cells, newly synthesized lipids must be selectively transported from their site of synthesis, typically the endoplasmic reticulum, to their target organelle or the plasma membrane.[2] The majority of intracellular lipid transfer is mediated by lipid transfer proteins (LTPs) at membrane contact sites.[3–5] Through their lipid selectivity, LTPs fine-tune organelle membrane composition, including the spatial distribution of signaling lipids.[6,7]

The steroidogenic acute regulatory protein-related (StAR) family comprises 15 soluble and membrane-associated LTPs,[8,9] three of which – STARD2, STARD7 and STARD10 – transfer phospholipids.[10–12] These proteins are known to transport phosphatidylcholine (PC), which in STARD2 and STARD7 is stabilized through interactions between the choline headgroup and an aromatic cage in the binding pocket.[13,14] STARD10 lacks this aromatic cage and can accommodate a broader spectrum of phospholipids, most notably phosphatidylethanolamine (PE) and phosphatidylglycerol (PG).[15,16] Although all three proteins are primarily cytosolic, STARD7 is initially targeted to mitochondria and also localizes to the mitochondrial intermembrane space.[17–19]

Despite these differences in structure and localization, the functional specialization of STARD2, STARD7 and STARD10 remains incompletely understood. Biochemical assays have demonstrated that STARD2 transports PC lipids at greatly varying rates depending on their acyl chain composition, suggesting that lipid selectivity may extend beyond headgroup recognition.[20] However, whether STARD2, STARD7 and

STARD10 exhibit distinct acyl chain selectivities, or are largely redundant, remains unclear. Equally unresolved is how lipid transfer activity is regulated. For STARD2, it is thought that two alpha-helices near the C-terminus mediate membrane association,[21,22] with phosphorylation initiating relocation to mitochondria.[23] In STARD10, phosphorylation of the C-terminal tail is thought to regulate transport activity.[24–26] The direct effects of these modifications on lipid binding and transfer have not been defined.

A central challenge in understanding LTP function is to distinguish what they can bind *in vitro* from what they actually carry in cells. Most studies have relied on *in vitro* reconstitution, incubating purified proteins with lipids to assess binding capacity.[27,28] Although such approaches have been instrumental in defining the lipid-binding preferences of STARD2,[20,29–31] STARD7[11,14] and STARD10,[15,32] they cannot capture binding selectivity within the spatially regulated cellular lipidome, where hundreds of lipid species compete for interaction. Similarly, while bifunctional and fluorescent lipids have proven powerful for studying protein–lipid interactions and lipid transport in cells,[12,33] currently available lipid probes represent only a fraction of the human lipidome.[34] To characterize endogenous protein–lipid interactions, LTPs have been affinity-purified from cells or tissues for analysis of co-purified lipids using thin-layer chromatography or mass spectrometry (MS),[35] as exemplified for STARD2 and STARD10.[16,36] However, studies addressing how acyl chains influence protein–lipid interactions are rare.[27] This represents a critical gap: acyl chain unsaturation significantly influences phospholipid transport kinetics and metabolic fate,[37] yet the endogenous lipid cargo of individual LTPs remains undefined at this level of resolution.

Here, we establish a multistage native MS workflow to directly identify endogenous ligands and regulatory post-translational modifications (PTMs) of human LTPs. We characterize lipid cargo with acyl-chain resolution by purifying STARD2, STARD7 and STARD10 from their native environment, separating intact protein–lipid complexes in the gas phase, and releasing endogenous ligands for identification. We uncover distinct and non-redundant acyl-chain selectivities among these phospholipid transfer proteins that align with tissue-specific expression patterns and lipid metabolic profiles. Integrating ligand profiling with top-down phosphorylation mapping and targeted mutation of the lipid-binding pocket, we define molecular mechanisms that regulate lipid selectivity and transfer. Together, our findings reveal a previously unrecognized alignment between acyl-chain–selective phospholipid transport, LTP regulation, and cellular lipid metabolism.

Results

Headgroup and acyl chain-selective phospholipid binding *in vitro*

To investigate the intrinsic phospholipid-binding preferences of STARD2, STARD7 and STARD10, we recombinantly expressed the proteins in *Escherichia coli* (**Figure S1**) and analyzed the purified products

using native MS. The native mass spectrum of STARD2 featured a single charge state distribution (*z* = 8–10+) comprising two species: i) ca. 30 % *apo* STARD2, and ii) 70 % STARD2 bound to an ensemble of ligands with an average molecular weight of 730 Da at a 1:1 ratio (**Figure 1a**). To characterize the copurified ligands, we isolated the protein–ligand complexes (*z* = 9+) in the ion trap of the mass spectrometer and activated them using higher-energy collisional dissociation (HCD) to release bound molecules for high-resolution mass analysis[38]. We subsequently assigned the released ions based on accurate mass and HCD fragmentation patterns (**Figure S2**). All copurified ligands belonged to the two most abundant phospholipid classes in *E. coli*, PE and PG, which have previously been observed to bind to STARD2 in the absence of PC.[31] In contrast, for STARD7 we could not detect evidence for phospholipid binding. Rather, the protein distribution consisted of two species, one corresponding to the expected mass of *apo* STARD7 and a second, more abundant species, shifted by +60 Da. (**Figure 1b**). We assigned the latter to an acetate adduct resulting from the ammonium acetate buffer (**Figure S3**). The lack of copurified phospholipids may indicate that STARD7 does not bind PE and PG, or alternatively, that the bacterial lipids are readily displaced by acetate upon buffer exchange into the native MS buffer. STARD10 purified almost exclusively as a 1:1 complex with phospholipids. The native mass spectrum showed >95 % STARD10 bound to PE and PG (**Figure 1c, Figure S2**). The increased amount of lipids copurified with STARD10 compared to STARD2 suggests that STARD10 has greater affinity for bacterial phospholipids.

To investigate competitive binding among different human phospholipid classes, we incubated purified STARD2, STARD7 and STARD10 with an equimolar mixture of dioleoyl (DO)PC, DOPE, DOPG, phosphatidylinostitol (DOPI), and phosphatidylserine (DOPS) (1:5 protein:lipid ratio). We then analyzed the bound lipids using the multistage native MS approach described above (**Figure 1a–c**). STARD2 bound exclusively to DOPC, which replaced all bacterial phospholipids, underscoring its high intrinsic affinity for PC. STARD7 bound to DOPC as well, albeit at low abundance, with most of the protein remaining in its *apo* or acetate-bound form. STARD10 bound not only to DOPC, but also to DOPE and DOPG in equal amounts. The bacterial phospholipids were not entirely replaced, again highlighting the high affinity of STARD10 for PE and PG.

In addition to lipid headgroup selectivity, we examined whether STARD2 and STARD10 preferentially copurified with bacterial phospholipids with specific acyl-chain compositions by comparing the acyl chain profile of copurifying phospholipids with total *E. coli* lipid extracts obtained from the same cell pellets (**Figure 1d**). For STARD2, we observed a strong positive correlation between the relative abundance of copurified lipids and their abundance in the bacterial membranes (Pearson's $r = 0.771$), implying minimal selection of specific acyl chains by the transporter. In contrast, the abundance of lipids that copurified with STARD10 were weakly correlated with the abundance of total lipids from STARD10-expressing cells (Pearson's $r = 0.021$). Specifically, STARD10 copurified with a relative excess of di-unsaturated lipids, notably PE and PG 36:2 and 34:2. This observation suggests intrinsic selectivity of STARD10 for phospholipids with unsaturations in both acyl chains.

Endogenous ligands reveal acyl chain selectivities

In their native cellular environment, the activity and cargo of LTPs is likely governed by factors beyond intrinsic lipid affinity, including phospholipid availability and spatial organization. Thus, to identify the endogenous ligands of STARD2, STARD7 and STARD10 we expressed the proteins with C-terminal FLAG tags in human HEK293S cells (**Figure S5**). The native mass spectrum of STARD2 showed that >95 % of the protein copurified with phospholipids, suggesting stronger binding to human than to *E. coli* lipids (70 %) (**Figure 2a**). We characterized these ligands using multistage native MS and found that they were exclusively PC lipids (**Figure 2b**, **Table S2**). Compared to the bulk HEK lipid extract, the copurified lipids were slightly enriched in di-unsaturated PC and clearly depleted in monounsaturated species, suggesting a moderate degree of acyl chain selectivity (**Figure S6**).

Next, full-length STARD7 was similarly expressed with its mitochondrial targeting sequence. The resulting native mass spectrum revealed mainly *apo* STARD7 with cleaved signal peptide and abundant 1:1 binding of acetate (+60 Da) as for the *E. coli* construct. Only a minor fraction (ca. 15%) of lipid-bound STARD7 was observed. Using native top-down MS, we localized the main signal peptide cleavage site between Ala78|Leu79 and found a minor isoform (ca. 25 %) cleaved between Ala77|Ala78 (**Figure S11**). Alternative cleavage of the STARD7 signal peptide has been reported previously but at an alternate site that we did not observe (Met76|Ala77).[18] Through isolation and activation of lipid-bound STARD7 complexes, we found that STARD7 copurified exclusively with PC lipids. The lipid abundance profile reflected their relative abundance in the whole-cell lipid extract, suggesting no significant acyl chain selectivity of STARD7 (**Figure S7**).

STARD10 expressed in HEK293S cells yielded a native mass spectrum that contained >95 % STARD10 bound to endogenous ligands. The pattern of peaks was complex, and repeated twice at intervals of 80 Da, suggesting phosphorylation of the protein (discussed below). Multistage measurements indicated that STARD10 copurified with PC, PE, plasmenyl PE (PE-P) and PG (**Figure S8**). PE (-P) and PG are therefore endogenous ligands of STARD10, consistent with our *in vitro* binding experiment and a recent LC-MS-based characterization of lipids associated with STARD10.[16] Interestingly, as also observed in *E. coli*, the predominant acyl chain combinations were di-unsaturated 36:2 and 34:2 phospholipids, while monounsaturated lipids were largely depleted. Based on our mass spectrometric characterization of phospholipids copurified with STARD2, STARD7 and STARD10 in HEK293S cells, we ranked the proteins according to their acyl chain selectivity from STARD7, which shows no lipid selectivity, over STARD2, which has moderate selectivity towards unsaturated lipids, to STARD10, which significantly enriches phospholipids carrying one unsaturation in each chain.

To expand our findings beyond HEK293S cells, which primarily contain monounsaturated PC lipids,[39] we also identified StARD cargo in HepG2 (hepatocellular carcinoma) cells, which contain higher levels of polyunsaturated PCs. The three StARD proteins expressed in HepG2 yielded comparable native mass spectra to their HEK293S counterparts, with some changes in copurified lipids (**Figures 2c, S6–8**). STARD2 enriched long, polyunsaturated lipids (C36-40) which are absent in HEK293S cells, while

monounsaturated PCs were clearly depleted. STARD7 showed no selectivity for specific lipids except a slight depletion of PC 34:1 and enrichment of PC 34:2. In contrast, the profile of PC lipids that copurified with STARD10 expressed in HepG2 cells only differed minimally from that expressed in HEK293S cells, highlighting the high intrinsic acyl chain selectivity of STARD10.

Given that the StARD phospholipid transporters copurify with PC species with distinct acyl chains, we hypothesized that they selectively extract these lipids from cellular membranes and may thereby influence cellular lipid equilibria. To investigate whether the expression levels of STARD2, STARD7 or STARD10 affected lipid metabolism, we analyzed whole-cell lipid extracts from HEK293S and HepG2 cells after 48 h of protein overexpression. Quantification of individual PC species revealed that overexpression of these LTPs modulated the overall cellular PC acyl-chain composition. (**Figure 3a)**. Lipid extracts of cells overexpressing STARD2 or STARD10 contained higher amounts of unsaturated PC species than cells overexpressing STARD7, which synthesized mainly monounsaturated PC at similar abundances to wild-type cells (**Figure S15**). Overexpression of individual LTPs resulted in a reproducible increase in their preferred PC species across both cell lines, highlighting a link between LTP expression levels and cellular lipid profiles.

We further investigated if overexpression of STARD2, STARD7 and STARD10 could also alter the acyl chain profiles of other phospholipids that are synthesized at the ER and share the same acyl-CoA pool as PC, most notably PE, PS and PI (**Figure S16, S17**). In the lipid extracts of HEK293S and HepG2 cells overexpressing the individual LTPs, we observed the most significant changes in the acyl chain composition of PI. Consistent with the observations made for PC, di- and polyunsaturated PI populations were significantly enhanced in cells overexpressing STARD2 or STARD10. Similar remodeling of PE was also observed, though these changes were not statistically significant in HEK293S cells. PS acyl chains were less affected, and PE-P and sphingomyelin showed no change. These observations are consistent with known lipid synthesis routes,[40] wherein PE-P pools undergo less acyl chain remodeling than PE and the sphingomyelin side chains are built from a different biosynthetic route than the glycerophospholipids. Taken together, we observe consistent trends in acyl chain remodeling depending on the expression levels of STARD2, STARD7 and STARD10 only for phospholipids that are closely linked to PC synthesis.

To assess the effect of the reverse condition, i.e., reduced LTP expression levels, we also performed lipidomic profiling following siRNA-mediated knockdown of each protein in HepG2 cells. After 72 h, we observed an approx. 3-fold reduction in LTP abundances in HepG2 cells (**Figure S18**). The cellular lipidomes only exhibited modest changes in PC species, with the most prominent differences observed between the control and the three knockdown conditions (**Figure S19**). In contrast, PE lipids were significantly affected. Most notably, we observed a reduction in polyunsaturated PE species upon STARD2 depletion compared to the three other conditions (**Figure S19**). This finding is consistent with our previous observation that overexpression of STARD2 increases the levels of polyunsaturated phospholipids. Polyunsaturated PC was also slightly depleted in STARD2 knockdown cells compared to the control, but the difference was not statistically significant. Overall, siRNA-mediated protein

knockdown produced more subtle changes in the lipidome than protein overexpression; however, together these data strongly indicate interactions between LTP expression levels and overall lipidomic profiles.

Given the relationship between LTP expression and cellular lipid composition, we hypothesized that LTP expression levels may correlate with lipid metabolism across tissues. We therefore examined whether LTP expression varies in accordance with the predominant lipid species produced in different organs. Based on gene expression data from the EMBL-EBI Expression Atlas,[41] *STARD7* RNA expression levels are largely invariant between human tissues, whereas *STARD2* and *STARD10* transcripts are selectively expressed in fewer regions, most notably in liver (**Figure 3b**). In line with the high expression levels of STARD2 and STARD10 in liver, a high percentage of their preferred lipid ligands, PC 34:2 and 36:2 and polyunsaturated PCs, was reported in human liver biopsies (**Figure S20**).[42,43] On the contrary, two independent studies on human heart sections (where STARD10 is expressed 10-fold less) did not detect any of the di-unsaturated PC lipids selectively bound by STARD10.[44,45] These data suggest that the acyl-chain selective LTPs STARD2 and STARD10 show higher expression levels in tissues with higher levels of PC unsaturation.

Role of a conserved arginine for lipid binding

Throughout our investigation, we observed that only a minor fraction of STARD7 copurified with lipids, even when expressed in human cell lines, and that the lipids were readily displaced by acetate. We also noted that acetate was only bound to the *apo* protein but not to the protein–lipid complex, suggesting that acetate competed with PC binding to STARD7. To investigate how lipid binding in STARD7 differs from STARD2 and STARD10, we considered the arginine residue located in the lipid binding pocket in a consensus sequence (YRKK/QWD) conserved in all three proteins (**Figure 4a**).[14] In the X-ray crystal structure of STARD2, this arginine contacts the phosphoryl group of PC ligands,[13] and in STARD7 it is crucial for phospholipid binding.[14] We expressed the three R→Q mutants STARD2 R78Q, STARD7 R189Q and STARD10 R92Q in *E. coli* and found by native MS that STARD7 R189Q did not bind PC, even when incubated with a large excess of DOPC (**Figure 4b**). Furthermore, we no longer observed acetate binding in the native mass spectrum (**Figure S3**). Arginine 189 is thus a key residue for both phospholipid and acetate binding in STARD7. Whether its ability to bind carboxylates such as acetate is relevant for the physiological function of STARD7 remains to be determined. By contrast native MS of STARD2 R78Q and STARD10 R92Q revealed that mutation of the arginine residue did not compromise phospholipid binding (**Figure 4b**, **Figure S4**). Together these findings suggest a different lipid binding mode in STARD7 compared to STARD2 and STARD10.

To gain further insights into the molecular mechanism behind these different binding profiles, we turned to all-atom molecular dynamics (AA-MD) simulations. We obtained structural models for DOPC-bound STARD2, STARD7 and STARD10, using Boltz-2[46] (**Figure 4c**). These simulations indicated that DOPC is highly mobile inside the cavity of STARD7 compared to STARD2 or STARD10, as highlighted by the

average root mean square fluctuation (RMSF) of the bound lipid (**Figure 4d**). Further analysis of the minimum distance between the conserved arginine and the phosphate headgroup of DOPC indicates that while this interaction was stably preserved throughout the simulation for STARD2 and STARD10, this was not the case for STARD7 (**Figure 4e**, dark traces). Mutation of the conserved arginine into a glutamine (R→Q mutation), affected the interaction between the DOPC phosphate group and the residue in all three cases, though STARD7 clearly showed the highest disruption with phosphate-glutamine distances reaching 1 nm (**Figure 4e**, light traces). Taken together, our data suggest that STARD7 has lower affinity for PC lipids compared to STARD2 and STARD10, and that, as a result, the R→Q mutation in STARD7 has a higher impact on PC binding when compared to STARD2 and STARD10. The predictions further confirmed preferential binding of acetate to the conserved Arg189 residue in STARD7, providing a rationale for the loss of carboxylate binding in the R→Q mutant (**Figure S22**).

Localization of phosphorylation sites in STARD2 and STARD10

For cytosolic LTPs, a crucial question is how they are targeted to specific membranes and how their activity is regulated. Previous studies have suggested that phosphorylation might play a key role in the regulation of STARD2 and STARD10.[23,26] To investigate such regulation, we set out to identify, quantify and localize phosphorylation and other PTMs on the three LTPs expressed in HEK293S cells. The measured mass of *apo* STARD2 was 42 Da higher than the expected mass, and we observed a peak shifted by 80 Da relative to the *apo* protein, suggesting partial phosphorylation (ca. 20 %) (**Figure 2b**). The +80 Da peak in the native mass spectrum could be removed by treatment with λ-phosphatase, confirming that the protein was partially phosphorylated (**Figure 5a**). To localize the phosphorylation site(s), we fragmented the protein in a native top-down experiment and used precisION[47] for fragment assignment and modification discovery (**Figure S9**). We found that all *b*-type sequence ions containing the N-terminus were shifted by 42.01 Da, confirming that STARD2 was entirely N-acetylated. Following enzymatic removal of the C-terminal FLAG tag, we were able to observe phosphorylated *y*-type ions stemming from the protein's C-terminus. We identified two phosphorylation sites each with ca. 10% occupancy: i) near the C-terminus and ii) at Ser185 (**Figure 5a**, **Figure S9**). A complementary proteomics analysis detected low-abundance phosphorylated peptides (2–3 % rel. to unmodified) containing the C-terminus and Ser185 (**Figure S10**). Intriguingly, Ser185 is located directly at the protein–membrane interface, close to the lipid entry site of STARD2, which is a prominent position to mediate membrane association and/or lipid entry.[22] To our knowledge, this is the first experimental evidence for STARD2 phosphorylation at this site.

For STARD7, we found no evidence of phosphorylation using either intact mass measurements or proteomics approaches. In contrast, native MS of STARD10 revealed an intact mass that exceeded the theoretical value by 202 Da. Using native top-down MS, we confirmed complete N-acetylation of STARD10 (**Figure S12**). Taking this PTM into account, the remaining mass shift of 160 Da could

correspond to two phosphorylation sites. Enzymatic treatment of the protein with λ-phosphatase confirmed our hypothesis: we obtained two new peaks corresponding to monophosphorylated and *apo* STARD10 (**Figure 5b**). STARD10 overexpressed in HEK293S or HepG2 cells is thus constitutively phosphorylated at two sites and has two additional phosphorylation sites that are partially occupied.

Proteomics analysis of STARD10 yielded two phosphorylated peptides, H229-R272 and M276-H322, which were 95% and 90% phosphorylated, respectively (**Figure S13**). Because native top-down MS did not yield fragments in the region of interest, we denatured the protein to obtain precursor ions with higher charge states that undergo more extensive fragmentation. We then activated the 28+ charge state using electron transfer dissociation with supplemental HCD (EThcD). For the doubly phosphorylated base peak, we clearly identified two phosphorylation sites, both 100 % occupied: Ser259 and Ser284 (**Figure S14**). Ser259 was previously identified as a constitutively phosphorylated site of STARD10 in breast epithelial cells,[24,25] and phosphorylation at Ser284 has been identified as an activity regulator in HEK293T cells.[26] Our results reveal that both sites are entirely phosphorylated under overexpression conditions. By fragmenting the proteoforms containing three and four phosphates, we confidently mapped the two partially occupied phosphorylation sites to the serine in the linker (GSG) and the C-terminus (TSLT). Accordingly, all phosphorylation sites detected here are in the flexible C-terminal region of STARD10 and can potentially serve as a regulatory mechanism to influence membrane association, lipid entry or yet uncharacterized protein–protein interactions.

Regulation of lipid transfer activity

Lastly, we sought to correlate our combined findings on acyl-chain selectivity, binding-pocket mutations, and phosphorylation with the lipid transfer activity of STARD2, STARD7 and STARD10 *in vitro*. We used a liposome assay based on resonance transfer between nitrobenzoxadiazole-PC (NBD-PC) and rhodamine-PE (Rh-PE) to measure the transfer of fluorescent NBD-PC between two types of liposomes (**Figure 6a**).[11] When donor and acceptor liposomes were mixed in the absence of LTPs, we observed a slow, linear increase in fluorescence, confirming that NBD-PC diffused from donor to acceptor liposomes. The maximum possible fluorescence that we used as a reference in the following measurements was obtained by adding Triton-X to the mixed liposomes.

In the first series of measurements, we hypothesized that the different acyl chain preferences of STARD2, STARD7 and STARD10 would lead to different lipid transfer kinetics of NBD-PC. We measured the initial transfer speed of NBD-PC 16:0-12:0 vs. 18:1-12:0 using catalytic protein concentrations to monitor the increase in fluorescence over 5 min (**Figure 6b**). In the absence of LTPs, both lipids exhibited comparable diffusion rates. In the presence of STARD2 or STARD10, however, the initial rate of lipid transfer was higher for the unsaturated NBD-PC 18:1-12:0, in agreement with our observed enrichment of unsaturated phospholipids. In contrast, STARD7 transported both NBD-PC probes at the same speed without preference. The results support our hypothesis that acyl chain preferences translate into differential lipid transfer kinetics.

Next, we investigated the lipid transfer abilities of the R→Q mutants (**Figure 6c**). The wild-type proteins expressed in *E. coli* significantly increased lipid transfer relative to passive diffusion of NBD-PC, though STARD7 expressed in *E. coli* was slightly less active than the version purified from HEK293S cells (**Figure S21**). The mutants STARD2 R78Q and STARD10 R92Q showed efficient PC transfer with minimally slower kinetics than the wild type. STARD7 R189Q, on the other hand, showed no lipid transfer activity. This finding consolidates our MS results which showed that lipid binding is abolished by point mutation of the arginine residue in the binding pocket of STARD7 but not STARD2 or STARD10.

To measure the impact of phosphorylation of STARD2 and STARD10 on lipid transfer, we compared the transport activity of non-phosphorylated STARD2 and STARD10 recombinantly expressed in *E. coli* with the transport activity of the proteins expressed in HEK293S cells (**Figure 6d**). For STARD2, we found no significant difference between the partially phosphorylated and non-phosphorylated protein. Either the phosphorylation did not affect the lipid transfer ability, or more likely the ratio of phosphorylated protein was too low to make the effect clearly visible. By contrast, phosphorylated STARD10 had a significantly reduced lipid transfer ability compared to the non-phosphorylated protein. To test if we could recover its lipid transfer ability by removing the phosphates, we treated STARD10 from HEK293S cells with λ-phosphatase and confirmed complete dephosphorylation by native MS. The phosphatase-treated STARD10 regained its lipid transfer activity, confirming that phosphorylation of STARD10 abolishes phospholipid transfer. This suggest that phosphorylation might indeed serve as a regulatory mechanism for lipid transfer.

Discussion

We describe a native MS-based approach to identify endogenous ligands of LTPs with acyl chain resolution, which we used to characterize the endogenous ligands of the human PC transfer proteins STARD2, STARD7 and STARD10. By isolating intact protein–lipid complexes from two human cell lines and identifying bound lipids using multistage native MS, we uncovered differential acyl chain selectivities of these three LTPs. We further determined PTMs and protein isoforms and related our findings to lipid transfer activity *in vitro*. Different from previous works using affinity purification and lipid extraction for LC-MS/MS, we preserve native protein–lipid interactions until their release in the gas phase, ensuring that all bound lipids are derived directly from intact protein–lipid complexes. Our approach requires no additional separation of proteins and lipids or controls, such as chromatographic retention times, while providing deep structural information on bound lipids including acyl chain identities.

While the acyl chain selectivity of STARD2 has been studied extensively, [20,30,31,36] it has not previously been compared to that of other major PC transporters including STARD7 and STARD10. Here we report clear differences in their acyl chain preferences, with STARD7 copurifying with a range of different PC lipids according to their natural abundance. By contrast STARD2 shows a clear preference for long, polyunsaturated chains according to our and previous reports,[20,30,31,36] and STARD10 reproducibly copurified with di-unsaturated phospholipids in different expression systems. Previously, STARD10 had been thought to select primarily monounsaturated lipids.[15] Our results show that those lipids are actually

depleted in favor of lipids with one unsaturation in each chain. Taken together, STARD2, STARD7 and STARD10 have evolved distinct acyl chain preferences, suggesting functional specialization within cells.

As LTPs mediate the majority of lipid transport in eukaryotic cells, the acyl chain-dependent differences in lipid transport kinetics must ultimately come down to preferences of LTPs for extracting and transporting lipids with certain chain length and saturation. For STARD2 and STARD10, which both prefer unsaturated lipids, this is likely related to the observation that intracellular transport of PC lipids occurs faster as the degree of unsaturation increases.[37] A possible explanation for the modulation of lipid abundances by LTP expression levels is that extraction of specific lipids by an LTP could stimulate further synthesis of the extracted lipid in the ER. This led us to hypothesize that the acyl chain-selective transport of lipids may exert a feedback control on lipid synthesis such that lipid levels are influenced by the expression levels of LTPs with different acyl chain selectivities (**Figure 7**). We observed stronger effects of protein levels on lipid metabolism under overexpression conditions than for siRNA-mediated knockdown. Because the silencing is gradual and the metabolic response is delayed, it is challenging to disentangle the individual processes involved. Nevertheless, the observed alterations in polyunsaturated PE upon STARD2 knockdown suggests that LTP expression levels impact cellular lipid metabolism.

The differential acyl chain selectivities of major cytosolic phospholipid transporters could have wider implications on lipid transport in different cell types. According to the EMBL-EBI Expression Atlas (http://www.ebi.ac.uk/gxa),[41] STARD7 is expressed at similar levels throughout human tissues, which could reflect its role as a non-selective PC transporter that is notably required for normal mitochondrial function.[33,49] On the other hand, the expression levels of STARD2 and STARD10 are highly tissue-dependent. Their acyl chain selectivities and distinct expression pattern could be linked by different lipids dominating different tissues (**Figure S20**). More generally, this points to a fine interplay between expression levels of LTPs and metabolism-dependent lipid distribution in specific tissues and cells.

We further addressed how lipid transfer activity of STARD2 and STARD10 may be regulated by reversible phosphorylation in cells. Phosphates introduce negative charges that can disrupt protein–membrane association and lipid extraction. We provide direct evidence that STARD10 is phosphorylated at up to four sites and that phosphorylation abolishes its lipid transfer activity in vitro. For STARD2, we did not detect phosphorylation of the previously reported putative protein kinase C-dependent phosphorylation site Ser110[23] but anticipate a regulatory role for the newly reported phosphorylation site at Ser185, which is located next to the lipid entry site.

Overall, our work establishes that the lipid binding preferences and structural modifications of LTPs are closely linked to their functional activity, supporting lipid binding as a meaningful indicator of transport capacity. In this context, native mass spectrometry emerges as a powerful approach to resolve lipid binding preferences and PTMs at molecular resolution. Looking ahead, an important next step will be to extend these insights beyond *in vitro* systems by directly relating lipid selectivity to differential lipid transport in living cells. This could be achieved using bifunctional PC species with defined acyl chains to monitor their intracellular transport as a function of LTP expression levels. Such experiments will

ultimately provide a comprehensive view of how LTP selectivity, expression levels and regulation shape lipid transport and metabolism.

Methods

Lipid standards

PC 18:1(9Z)/18:1(9Z) (DOPC), PE 18:1(9Z)/18:1(9Z) (DOPE), PG 18:1(9Z)/18:1(9Z) (DOPG), PS 18:1(9Z)/18:1(9Z) (DOPS) and PI 18:1(9Z)/18:1(9Z) (DOPI) were purchased from Avanti Research, dissolved in chloroform, and dried overnight in a centrifugal evaporator. The lipid films were resuspended to a final concentration of 5 mM by sonication in 200 mM ammonium acetate containing 2× critical micelle concentration (CMC) C8E4. 16:0-12:0 NBD-PC, 16:0-12:0 NBD-PC and 16:0-16:0 Rhodamine-PE were purchased from Avanti Research and dissolved in chloroform at a final concentration of 1 nmol/µL.

Expression of STARD2, STARD7 and STARD10 in *E. coli*

Codon-optimized double-stranded DNA fragments encoding STARD2, STARD2 R78Q, STARD7 (76–370), STARD7 (76-370) R189Q, STARD10, and STARD10 R92Q was inserted into a modified pET28b vector using Gibson assembly, resulting in a consturct encoding the respective protein with an N-terminal 6×His tag, maltose binding protein (MBP) and TEV protease cleavage site. The plasmids were transformed into *E. coli* C43(DE3) cells (New England Biolabs). Overnight cultures were grown with shaking in Luria Broth under kanamycin selection (50 µg/mL) at 37 °C. 10 mL of the overnight cultures was used to inoculate 1 L of expression culture. The cultures were grown at 37 °C to OD_{600} = 0.5 and induced by the addition of IPTG to a final concentration of 0.5 mM. Induced cultures were shaken at 30 °C for 4 h. Cell pellets were harvested by centrifugation at 5000 × g for 15 min.

The cells were resuspended in 20 mL lysis buffer (50 mM Tris pH 8.0, 300 mM NaCl, 2.5 mM beta-mercaptoethanol (BME)) per liter of culture using one EDTA-free protease inhibitor tablet (Roche) per 50 mL lysis buffer. The cells were disrupted by four passes through a microfluidizer (30,000 psi) and centrifuged at 20,000 × g for 20 min. The lysate was filtered through a 0.45 µm syringe filter before loading onto a 5-mL Ni-NTA column equilibrated with five column volumes (CV) of wash buffer (20 mM Tris pH 8.0, 300 mM NaCl, 20 mM imidazole, 2.5 mM BME). The column was washed with 10 CV wash buffer, before the protein was eluted with 5 CV elution buffer (20 mM Tris pH 8.0, 300 mM NaCl, 300 mM imidazole, 2.5 mM BME). The elutate was dialyzed overnight with TEV protease against dialysis buffer (20 mM Tris pH 8.0, 150 mM NaCl, 2.5 mM BME). STARD proteins were separated from TEV protease and MBP by reverse Ni-NTA affinity column chromatography. The proteins were further purified over a Superdex 200 10/300 Increase gel filtration column equilibrated in 20 mM Tris pH 8.0, 100 mM NaCl, 2.5 mM BME.

Expression of STARD2, STARD7 and STARD10 in human cell lines

HEK293S and HepG2 cell lines stably expressing Tet repressor protein (TetR) were generated by lentiviral transduction and blasticidin selection (2 µg/mL).[50] The cells were adherently grown in DMEM/F-12 medium supplemented with non-essential amino acids, 10 % FBS and blasticidin (2 µg/mL). Vectors containing full-length STARD2, STARD7 or STARD10 with a C-terminal FLAG tag separated by an IRES site from a GFP reporter protein were brought into the cells by lentiviral transduction. After a week of culturing, the cells were sorted for GFP expression using FACS.

For protein expression in HEK293S TetR cells, the cells were suspension-adapted and grown in Freestyle medium supplemented with 1 % FBS. Protein expression was induced by the addition of tetracycline hydrochloride (1 µg/mL) to a 1 L culture after a cell density of 2–3 million cells/mL was reached. 24 h after induction, sodium butyrate was added (5 mM), and expression was allowed to proceed for another 24 h. 48 h after induction, the cells were harvested by centrifugation (300 × g) and washed twice with PBS.

For protein expression in HepG2 TetR cells, each cell line was expanded into twelve 150 mm dishes containing 25 mL complete media. At 80 % confluency, protein expression was induced by the addition of tetracycline hydrochloride (1 µg/mL). After 24 h, 5 mM sodium butyrate was added, and the cells were harvested by scraping 48 h after induction. The cell pellet was washed twice with PBS.

Proteins were purified using anti-FLAG magnetic agarose beads (Thermo Fisher Scientific). Cell pellets were resuspended in 50 mL lysis buffer (50 mM HEPES pH 8.0, 150 mM NaCl, 5 % glycerol) with a protease inhibitor tablet and stirred for 1 h. The cells were lyzed in a Potter-Elvehjem homogenizer, and cell debris was cleared by centrifugation at 10,000 × g for 10 min and 20,000 × g for 20 min. The supernatant was filtered through a 0.45 µm syringe filter before adding 250 µL magnetic beads that were previously washed with 2 x 1mL lysis buffer. The suspension was placed on a roller for 1 h to allow protein binding to the beads. The supernatant was removed, and the beads were washed 3 x with 5 mL and 10 × with 1 mL lysis buffer (total wash volume: 25 mL). For elution, 0.5 mL of 1× FLAG peptide (DYKDDDDK; 1 mg/mL) in lysis buffer was added to the beads and placed on a roller for 30 min. The elution was repeated once. The resulting 1 mL eluate was concentrated to 100 µL using 10 kDa MWCO spin filters and washed twice by centrifugation with 0.5 mL lysis buffer to remove FLAG peptide.

Lipid extraction

Lipids were extracted from the cell pellets of bacterial and human cells obtained at the end of the protein expression, following the Bligh-and-Dyer protocol.[51] Briefly, ca. 20 mg of the cell pellet was resuspended in 0.8 mL aqueous buffer (20 mM Tris pH 8.0, 150 mM NaCl) in a glass vial and mixed with 2 mL methanol and 1 mL chloroform. After sonication for 10 min, 1 mL chloroform and 1 mL of the buffer were added and the mixture was vortexed for 30 s. After centrifugation at 1000 × g for 10, the lower (chloroform) phase was transferred into a clean glass vial. The solution was directly analyzed by MS or dried for the generation of liposomes.

***In vitro* lipid binding assays**

To determine lipid binding preferences *in vitro*, STARD2, 7 and 10 (20 µM) expressed in *E. coli* were incubated with a 1:1:1:1:1 mixture containing DOPC, DOPE, DOPG, DOPS and DOPI (100 µM total lipid concentration) in 200 mM ammonium acetate containing 2xCMC C8E4. After 5 min incubation, the proteins were buffer-exchanged into 200 mM ammonium acetate using BioSpin-6 columns (BioRad) to remove excess lipids. Protein-lipid complexes were analyzed by native MS and MS^2 experiments in positive and negative ion modes to release and assign bound lipids based on exact mass.

Native mass spectrometry

Native MS was performed on an Orbitrap Eclipse Tribrid mass spectrometer (Thermo Fisher Scientific). Proteins were buffer-exchanged into native MS buffer (200 mM ammonium acetate pH 7.0) using BioSpin-6 columns (BioRad). Proteins were ionized by nano electrospray ionization using gold-coated borosilicate capillaries pulled in-house using a P97 Micropipette Puller (Sutter Instrument Corporation) and coated with an AgarAuto Sputter Coater.

STARD proteins were analyzed in Intact Protein mode using the Orbitrap for mass analysis (typically *m/z* 1,000–6,000, resolution = 15,000 @ *m/z* 200). For the identification of copurified phospholipids, the intact protein–lipid complexes were isolated with a wide isolation window (usually 100 Th) in the ion trap (STARD2: *m/z* 2950 (10+); STARD7: *m/z* 3230 (12+); STARD10: *m/z* 3130 (12+), *m/z* 3760 (10−)) and activated using HCD (6–20 % NCE). MS^2 spectra of released lipids were recorded in the Orbitrap at high resolution (*m/z* 500–1,000, resolution = 500,000 @ *m/z* 200). For lipid identification, MS^3 spectra were recorded in the ion trap using HCD (25–30 % NCE) to identify lipid class and acyl chains. Lipid extracts were analyzed by direct infusion in Small Molecule mode. Mass spectra of lipids were recorded in the Orbitrap at high resolution (500,000 @ *m/z* 200) in triplicate.

For native top-down experiments, apo proteins were isolated in the ion trap and fragmented using HCD (70–100 V). Fragment spectra were recorded in the Orbitrap at high resolution (240,000 @ *m/z* 200). STARD10 was denatured by adding an equal volume of a solution containing 90 % acetonitrile and 10 % isopropanol with 2 % formic acid. The 28+ charge state was isolated using a narrow isolation window (±1 Th) to select individual phosphorylation states. Isolated ions were fragmented using EThcD (Reaction time: 1.5 ms, 30 % CE), and fragment spectra were recorded in the Orbitrap at high resolution (240,000 @ *m/z* 200). Fragment ions were assigned using precisION[47] with a 3 ppm (post-calibration) matching tolerance.

Lipid identification

Lipids that copurified with STARD2, STARD7 and STARD10 were identified based on MS^3 HCD/HCD spectra. PC lipids were detected in positive ion mode and assigned through diagnostic headgroup fragments (*m/z* 184.07). Acyl chains were assigned based on low-intensity fragments resulting from neutral loss of each chain. PE and PG were detected in negative ion mode and assigned based on carboxylate fragments.

Lipid quantification

To quantify changes in the acyl chain profiles of phospholipids in whole-cell lipid extracts, we extracted their intensities from high-resolution mass spectra in triplicate and normalized within each lipid class. Statistical analyses were performed on groups of lipids containing one or two double bonds using one-way analysis of variance (ANOVA). Pairwise comparisons were conducted using Tukey's Honest Significant Difference test. In addition, pairwise Welch's t-tests were applied to all condition pairs, and resulting p-values were corrected for multiple testing using the Benjamini–Hochberg false discovery rate (FDR) procedure. For lipid classes containing one, two, or more than two double bonds, overall compositional differences were assessed using PERMANOVA based on Aitchison distances, and group dispersion was tested with a permutation-based beta-dispersion analysis. For each feature, one-way ANOVA was performed to test for condition effects, followed by pairwise contrasts between conditions. The resulting p-values were adjusted using the Benjamini–Hochberg procedure, and the adjusted values (q-values) were used to determine statistical significance (threshold $q < 0.05$).

siRNA-mediated protein knockdown

For knockdown of LTPs in HepG2 cells, we used ON-TARGETplus SMART pool siRNA specifically targeting STARD2, STARD7 and STARD10 (Dharmacon). The siRNA pools contained the following target sequences: STARD2: GGAAGUGGCAUUUCGUUCA, UGAUCCGGGUGAAGCAAUA, CGAUCGAGAGUGACGGCAA, CAAACUGGAUGACGUGCCA; STARD7: CAUCGAUUGUGCAGCGCUU, CCUCUGAGCGAAAGAACGA, UUAAUGAGAUGAAGCGGUU, CCAAUGUACUCACGGGAUU; STARD10: GGAAAGACUUGGUCCGAGC, GACAUUGAGUACCGCAAGA, AGAGCAGAGAGGAGCGGAU, GCCCGAUGACCAAGACUUU. HepG2 cells were seeded into 12-well plates at a seeding density of 10^5 cells per well. After overnight incubation in complete medium (DMEM/F-12 medium supplemented with non-essential amino acids, 10 % FBS), the medium was replaced by 1 mL of transfection solution containing siRNA at a final concentration of 50 nM and 4 µL DharmaFECT 4 transfection reagent per well. According to the manufacturer's instructions, siRNA and transfection reagent were first incubated in a 200 µL volume for 20 min in serum-free medium before 800 µL complete medium was added. The transfections were performed in six replicates for each protein and controls. Control cells were incubated with transfection reagent under identical conditions without adding siRNA. Cells were incubated with transfection solution at 37 °C with 5 % CO_2 for 72 h. Cells were washed twice with PBS, harvested by cell scraping, and prepared for lipid analysis and proteomics.

Data-independent acquistion proteomics

For proteomics, ca. 6×10^5 cells were lyzed in 46 µL lysis buffer (5 % SDS in 50 mM Tris-HCl, pH 7.4) through sonication. After clarification by centrifugation (13,000 × g, 8 min), the supernatant was transferred into a new tube. 2 µL of TCEP (120 mM in water) was added and the reduction was allowed to proceed for 15 min at 55 °C. After incubation with 2 µL iodoacetamide (250 mM in 50 mM Tris-HCl) for 10 min at room temperature, the solution was acidified with 10 µL phosphoric acid (12 % in water).

350 µL wash buffer (100 mM Tris-HCl in 90 % methanol) was added, and the solution was applied to a miniprep column. Proteins were bound to the column by centrifugation (4000 × g, 30 s). The column was washed four times with 400 µL wash buffer through centrifugation and dried by a final centrifugation at 4000 × g for 1 min before being transferred into a new tube. 125 µL digestion buffer was applied to the column (50 mM Tris containing a total of 2 µg trypsin per column). Proteins were digested overnight at 37 °C. Peptides were eluted sequentially with 50 mM Tris, 0.2 % formic acid in water, and 50 % acetonitrile in water through centrifugation (4000 × g, 1 min; 80 µL per elution). The eluates were combined and dried in a centrifugal evaporator. The dried peptides were resuspended in 0.1 % formic acid and diluted to a final concentration of 100 ng/µL.

Purified peptides were separated via nanoflow reversed-phase liquid chromatography (nanoElute 2, Bruker Daltonics) with a 30 min gradient. Peptides (50 ng, 0.5 µL injection volume) were loaded directly onto a 25 cm × 75 µm column packed with 1.7 µm C18 beads (pore size 120 Å; Aurora Ultimate CSI, IonOpticks) and separated at a flow rate of 250 nL/min and a column temperature of 50°C. Mobile phase A consisted of 0.1% formic acid in water, and mobile phase B consisted of 0.1% formic acid in acetonitrile (v/v; Fisher Scientific, LC-MS grade). The gradient was as follows: 2–23% B over 18 min, 23–35% B over 4 min, and 35–90% B over 4 min, followed by a 4-min wash at 90% B. Eluting peptides were infused into a TIMS quadrupole time-of-flight mass spectrometer (timsTOF Ultra, Bruker Daltonics) equipped with an electrospray ion source (CaptiveSpray, Bruker Daltonics). Source parameters were set to a capillary voltage of 4,500 V, a dry gas flow of 3.0 L min^{-1}, and a dry gas temperature of 180 °C. Data was acquired in dia-PASEF mode over an *m/z* range of 400–1,000 and an ion mobility range of $1/K_0$ = 0.64–1.45 Vs/cm^2 (**Table S4**). The TIMS analyzer was operated at a 100% duty cycle with 100 ms accumulation and 100 ms ramp times (acquisition cycle time = 0.96 s). Collision energies were linearly stepped from 20 to 59 eV as a function of increasing ion mobility.

dia-PASEF raw files were processed using the “DIA_SpecLib_Quant_diaPASEF” workflow in FragPipe v.23.1.[52,53] Pseudo-MS/MS spectra were generated using diaTRACER v.1.3.3 and searched using MSFragger v.4.3. Searches were performed against the Homo sapiens UniProt reference proteome (UP000005640; reviewed entries only) supplemented with common contaminants and decoys (downloaded November 2025). Precursor and fragment mass tolerances were set to 20 ppm, and the isotope error window was set to 0/1/2. Mass calibration and parameter optimization were enabled. Enzymatic specificity was set to “stricttrypsin”, allowing up to two missed cleavages. Carbamidomethylation of cysteine was specified as a fixed modification, while methionine oxidation, protein N-terminal acetylation, and pyro-Glu/Gln formation at peptide N-termini were included as variable modifications (maximum of three variable modifications per peptide). MSBooster and Percolator were used to predict retention time and MS/MS spectra, and to rescore peptide–spectrum matches (PSMs). PSMs were filtered to a 1% false-discovery rate (FDR) and combined with the pseudo-MS/MS spectra using EasyPQP v.0.1.52 to generate a spectral library for DIA quantification (139,376 precursors mapping to 8,002 protein groups).

dia-PASEF runs were quantified using DIA-NN v.1.8.2 beta 8 with the spectral library generated in FragPipe. Mass accuracy settings for MS1 and MS2, as well as the scan window, were determined automatically by DIA-NN based on the first run in the experiment. Precursor and protein group identifications were filtered at 1% FDR. Protein inference was disabled, retaining protein group assignments from the input spectral library. Quantification was performed using fixed-width peak-centre integration. Cross-run normalisation was performed using DIA-NN's default RT-dependent method, and protein group quantities were calculated using the MaxLFQ algorithm. Quantification matrices for precursors, protein groups, and gene groups were exported with 1% FDR filtering. The abundance of STARD2, STARD7 and STARD10 were quantified in six replicates per condition (control and three siRNA knockdown conditions). p-values were determined by pairwise Welch's t-test between the control sample and each knockdown condition, using Bonferroni correction to correct for multiple testing. The mass spectrometry proteomics data have been deposited to the ProteomeXchange Consortium via the PRIDE[54] partner repository with the dataset identifier PXD072869.

Quantiative phosphoproteomics

Proteomics analysis of purified STARD2, STARD7 and STARD10 expressed in HEK293S cells was performed after tryptic digestion of coomasie-stained gel slices. Briefly, the gel pieces were dehydrated and washed, then treated with 10 mM DTT in 25 mM ammonium bicarbonate for 1 h at 56 °C, followed by a 45 min reaction at room temperature in the dark with 55 mM iodoacetamide in 25 mM ammonium bicarbonate. After washing, the gel pieces were incubated overnight at 37 °C with 25 ng/µL trypsin in 25 mM ammonium bicarbonate. The peptide-containing supernatant and wash were combined and dried in a centrifugal evaporator. The peptides were redissolved by sonication in 20 µL LC-MS grade water containing 0.1 % formic acid.

Purified peptides were separated by nanoflow reversed-phase HPLC (Dionex UltiMate 3000 system) with a 60 minute gradient. Peptides (1 µL) were loaded onto a 75 µm x 2 cm pre-column, followed by an analytical C18 column (Acclaim PepMap 100, C18, 75 µm x 15 cm, Thermo Scientific), which was coupled to an Orbitrap Eclipse Tribrid mass spectrometer. Mobile phase A consisted of 0.1 % formic acid in water, and mobile phase B consisted of 80 % acetonitrile, 20 % water and 0.1 % formic acid (v/v, Fisher Scientific, LC-MS grade). Buffer B was gradually increased from 5 to 40 % over 45 min, followed by 40 to 99 % over 5 min, where it was maintained for an additional 5 min. The mass spectrometer was operated in data-dependent acquisition mode including charge states 2–5 and with an exclusion duration of 30 s. Full MS scans were recorded from m/z 300–2000 at a resolution of 120,000, and MS^2 scans were recorded with HCD (30 % NCE) at a resolution of 30,000. Data was analyzed using Fragpipe with quantification from IonQuant.[55]

Structure prediction and system setup for molecular dynamics simulations

All wildtype structures were predicted using Boltz-2.[46] Where applicable, available crystallographic structures were incorporated as templates to guide the prediction. The inclusion of DOPC as a ligand

was achieved by adding its associated SMILES representation as input for Boltz-2. Mutant structures were generated from the predicted wildtype structures by converting the conserved arginine into a glutamine using Chimera.[56] To predict the structure of STARD2, the full-length sequence from UniProt accession Q9UKL6 was used as input, supplying PDB ID: 1LN1 as a structural template. For STARD10, the full-length sequence from UniProt accession Q9Y365 and the PDB ID: 6SER were used as sequence input and structural template, respectively. For STARD7, Uniprot: Q9NQZ5, the sequence was truncated to begin from residue number 76 to account for the signal peptide cleavage. The respective mutants for STARD2, STARD7, and STARD10 were R78Q, R189Q (in reference to the full-length numbering of the residues), and R92Q. The predictions' confidence scores were 0.957, 0.799, and 0.855 for the DOPC-bound wildtype STARD2, STARD7 and STARD10, respectively. To build each system, the predicted DOPC-bound protein was placed in a 10 nm cubic box, which was then solvated with water and a 0.15 M concentration of NaCl.

Molecular dynamics simulations

The CHARMM36m force field[57] was used in combination with the GROMACS (v 2023.3) package[58]. The topology was generated using GROMACS pdb2gmx. The systems were equilibrated following the CHARMM-GUI six-step protocol[59]. Each system was initially minimized for 5,000 steps. Next, two equilibrations in the NVT ensemble were run for 125 ps, followed by four equilibrations in the NPT ensemble, gradually removing the constraints on the protein backbone and lipid head. For the production runs, a time step of 2 fs was used with the md integrator. Three independent replicas were simulated for 2 μs each. Temperature was kept at 310 K using a V-rescale thermostat,[60] while pressure was maintained at 1 bar using an isotropic C-rescale barostat[61]. A verlet cutoff scheme with a cutoff value of 1.2 nm was used to calculate van der Waals and coulombic interactions. Beyond 1.2 ns, particle mesh Ewald was used to compute long-range interactions. Hydrogen bonds were constrained using the LINCS algorithm[62].

Simulation analysis

To calculate the Root Mean Square Fluctuation (RMSF) of DOPC in the protein cavity, GROMACS's gmx rmsf was used, omitting the hydrogens to reduce noise. To calculate the minimum distance between the phosphate atom and the arginine/glutamine residue, gmx mindist was used. The line plots show the average values from the three replicas for each system with the shaded region showing the standard mean of error with respect to each individual replica. The probability density plots were calculated for only the last 1800 ns of the simulations' durations, using Matplotlib's histogram function. All graphical plots were generated using Matplotlib[63]. All visual representations were created using VMD[64].

Desphosphorylation of STARD2 and STARD10

To dephosphorylate STARD2 and STARD10 expressed in HEK293S cells, 20 μL of the purified protein (90 μM) was incubated with 0.8 μL λ protein phosphatase (New England Biolabs) and 2 μL $MnCl_2$ (10 mM)

in the presence of 1 mM DTT. For dephosphorylation of STARD2 and partial dephosphorylation of STARD10, the reaction mixture was incubated for 1 h at 30 °C before buffer exchange into ammonium acetate for native MS. To completely dephosphorylate of STARD10, the incubation time was increased to 4 h at room temperature.

Liposome preparation for lipid transfer assay

Protein-mediated lipid transfer between two populations of liposomes was measured based on Förster resonance energy transfer between NBD-PC and Rh-PE.[65,66] Acceptor liposomes were generated from dried HEK293S lipid extract. For the generation of donor liposomes, we determined the mass of the dried lipid extract and added NBD-PC and Rh-PE to a final concentration of 1 and 5 mol%, respectively (assuming an average molecular weight of 750 g/mol). The lipid film supplemented with fluorescent lipids was redissolved in chloroform, vortexed, and dried again. The dried lipid films were reconstituted in warm (37 °C) liposome buffer (20 mM Tris pH 8.0, 150 mM NaCl) at a final lipid concentration of 500 nmol/mL. Liposomes were generated by extrusion of the suspension through a mini extruder (Avanti Research) using polycarbonate membranes with pore sizes decreasing from 400 nm to 200 nm and finally 100 nm.

Lipid transfer assay

The lipid transfer assay was performed in a 96-well plate at 25 °C in a total volume of 200 µL using a plate reader (Clariostar; BMG Labtech). The excitation wavelength was 464±5 nm, and emission was measured at 530±5 nm. Fluorescence was measured in time steps of 15 s, after initial shaking of the plates for 10 s. Control measurements were performed in triplicate for solutions containing either 15 µL donor liposomes, 30 µL acceptor liposomes, or 15 µL donor liposomes with 30 µL acceptor liposomes with and without 1 % Triton-X. The average fluorescence measured with the addition of Triton-X was set as the maximum fluorescence. To measure the lipid transfer activity of STARD proteins, 5 µL of the protein (10 µM; final concentration = 0.25 µM) was mixed with 15 µL donor liposomes in 150 µL liposome buffer. 30 µL acceptor liposomes were added and the measurement was started 30 s after the addition. To measure the initial lipid transfer kinetics for NBD-PC with different acyl chains, the proteins were added at reduced concentrations: STARD2 0.05 µM, STARD7 0.25 µM, STARD10 0.10 µM. All measurements were performed in triplicate, and the data were normalized against the maximum fluorescence.

Declarations

Acknowledgements

This work was financially supported by a Wellcome Trust grant (221795/Z/20/Z; C.V.R.) and the Leopoldina fellowship program of the German National Academy of Sciences Leopoldina (LPDS 2023-07; C.K.). S.V acknowledges support from the Swiss National Science Foundation (grant CR00I5-236020), and from the European Research Council under the European Union's Horizon 2020 research

and innovation program (grant agreement no. 803952). This work was supported by grants from the Swiss National Supercomputing Centre under project IDs lp24 and lp69.

Author contributions

C.K. and C.V.R. designed the project. Cloning, bacterial expression and protein purification were carried out by C.K. Human cell lines were established by C.K., S.A.S. and T.E.-B. C.K. and J.L.B. collected native MS data. C.K., J.L.B. and O.B.R. performed proteomics and data analysis. Y.A. and S.V. executed and analyzed molecular dynamics simulations. All authors discussed the results and commented on the manuscript.

Competing interests

The authors have no competing interests to declare.

Data availability

Supplementary figures and tables are provided in the Supporting Information. Raw files are accessible via Figshare. The mass spectrometry proteomics data have been deposited to the ProteomeXchange Consortium via the PRIDE[54] partner repository with the dataset identifier PXD072869.

References

1. van Meer, G., Voelker, D. R. & Feigenson, G. W. Membrane lipids: where they are and how they behave. *Nat. Rev. Mol. Cell Biol.* **9**, 112–124 (2008).
2. Reinisch, K. M., De Camilli, P. & Melia, T. J. Lipid Dynamics at Membrane Contact Sites. *Annu Rev Biochem* **94**, 479–502 (2025).
3. Wong, L. H., Copic, A. & Levine, T. P. Advances on the Transfer of Lipids by Lipid Transfer Proteins. *Trends Biochem Sci* **42**, 516–530 (2017).
4. Wong, L. H., Gatta, A. T. & Levine, T. P. Lipid transfer proteins: the lipid commute via shuttles, bridges and tubes. *Nat. Rev. Mol. Cell Biol.* **20**, 85–101 (2019).
5. Reinisch, K. M. & Prinz, W. A. Mechanisms of nonvesicular lipid transport. *J. Cell Biol.* **220** (2021).
6. Pemberton, J. G., Kim, Y. J. & Balla, T. Integrated regulation of the phosphatidylinositol cycle and phosphoinositide-driven lipid transport at ER-PM contact sites. *Traffic* **21**, 200–219 (2020).
7. Lipp, N. F., Ikhlef, S., Milanini, J. & Drin, G. Lipid Exchangers: Cellular Functions and Mechanistic Links With Phosphoinositide Metabolism. *Front Cell Dev Biol* **8**, 663 (2020).
8. Alpy, F. & Tomasetto, C. START ships lipids across interorganelle space. *Biochimie* **96**, 85–95 (2014).
9. Clark, B. J. The START-domain proteins in intracellular lipid transport and beyond. *Mol Cell Endocrinol* **504**, 110704 (2020).
10. Kanno, K., Wu, M. K., Scapa, E. F., Roderick, S. L. & Cohen, D. E. Structure and function of phosphatidylcholine transfer protein (PC-TP)/StarD2. *Biochim Biophys Acta* **1771**, 654–662 (2007).

11. Horibata, Y. & Sugimoto, H. StarD7 mediates the intracellular trafficking of phosphatidylcholine to mitochondria. *J. Biol. Chem.* **285**, 7358–7365 (2010).
12. Haberkant, P. *et al.* In vivo profiling and visualization of cellular protein-lipid interactions using bifunctional fatty acids. *Angew. Chem. Int. Ed.* **52**, 4033–4038 (2013).
13. Roderick, S. L. *et al.* Structure of human phosphatidylcholine transfer protein in complex with its ligand. *Nat Struct Biol* **9**, 507–511 (2002).
14. Bockelmann, S. *et al.* A search for ceramide binding proteins using bifunctional lipid analogs yields CERT-related protein StarD7. *J. Lipid Res.* **59**, 515–530 (2018).
15. Olayioye, M. A. *et al.* StarD10, a START domain protein overexpressed in breast cancer, functions as a phospholipid transfer protein. *J. Biol. Chem.* **280**, 27436–27442 (2005).
16. Titeca, K. *et al.* A system-wide analysis of lipid transfer proteins delineates lipid mobility in human cells. *bioRxiv* (2024).
17. Saita, S. *et al.* PARL partitions the lipid transfer protein STARD7 between the cytosol and mitochondria. *EMBO J.* **37** (2018).
18. Horibata, Y. *et al.* Identification of the N-terminal transmembrane domain of StarD7 and its importance for mitochondrial outer membrane localization and phosphatidylcholine transfer. *Sci. Rep.* **7**, 8793 (2017).
19. Saita, S. *et al.* PARL mediates Smac proteolytic maturation in mitochondria to promote apoptosis. *Nat. Cell Biol.* **19**, 318–328 (2017).
20. Kasurinen, J., Van Paridon, P. A., Wirtz, K. W. & Somerharju, P. Affinity of phosphatidylcholine molecular species for the bovine phosphatidylcholine and phosphatidylinositol transfer proteins. Properties of the sn-1 and sn-2 acyl binding sites. *Biochemistry* **29**, 8548–8554 (1990).
21. Feng, L., Chan, W. W., Roderick, S. L. & Cohen, D. E. High-level expression and mutagenesis of recombinant human phosphatidylcholine transfer protein using a synthetic gene: evidence for a C-terminal membrane binding domain. *Biochemistry* **39**, 15399–15409 (2000).
22. Talandashti, R., Moqadam, M. & Reuter, N. Model Mechanism for Lipid Uptake by the Human STARD2/PC-TP Phosphatidylcholine Transfer Protein. *J. Phys. Chem. Lett.* **15**, 8287–8295 (2024).
23. de Brouwer, A. P. *et al.* Clofibrate-induced relocation of phosphatidylcholine transfer protein to mitochondria in endothelial cells. *Exp. Cell Res.* **274**, 100–111 (2002).
24. Olayioye, M. A. *et al.* The phosphoprotein StarD10 is overexpressed in breast cancer and cooperates with ErbB receptors in cellular transformation. *Cancer Res.* **64**, 3538–3544 (2004).
25. Hoffmann, P. *et al.* Breast cancer protein StarD10 identified by three-dimensional separation using free-flow electrophoresis, reversed-phase high-performance liquid chromatography, and sodium dodecyl sulfate-polyacrylamide gel electrophoresis. *Electrophoresis* **26**, 1029–1037 (2005).
26. Olayioye, M. A. *et al.* Phosphorylation of StarD10 on serine 284 by casein kinase II modulates its lipid transfer activity. *J. Biol. Chem.* **282**, 22492–22498 (2007).

27. Hamai, A. & Drin, G. Specificity of lipid transfer proteins: An in vitro story. *Biochimie* **227**, 85–110 (2024).
28. Saliba, A. E., Vonkova, I. & Gavin, A. C. The systematic analysis of protein-lipid interactions comes of age. *Nat. Rev. Mol. Cell Biol.* **16**, 753–761 (2015).
29. Kamp, H. *et al.* Specificity of the phosphatidylcholine exchange protein from bovine liver. *Biochemistry* **16**, 1310–1316 (1977).
30. Somerharju, P. J., Van Loon, D. & Wirtz, K. W. Determination of the acyl chain specificity of the bovine liver phosphatidylcholine transfer protein. Application of pyrene-labeled phosphatidylcholine species. *Biochemistry* **26**, 7193–7199 (1987).
31. de Brouwer, A. P. *et al.* The binding of phosphatidylcholine to the phosphatidylcholine transfer protein: affinity and role in folding. *Chem Phys Lipids* **112**, 109–119 (2001).
32. Carrat, G. R. *et al.* The type 2 diabetes gene product STARD10 is a phosphoinositide-binding protein that controls insulin secretory granule biogenesis. *Mol Metab* **40**, 101015 (2020).
33. Zhang, J. *et al.* De novo labeling and trafficking of individual lipid species in live cells. *Mol Metab* **61**, 101511 (2022).
34. Peng, T., Yuan, X. & Hang, H. C. Turning the spotlight on protein-lipid interactions in cells. *Curr. Opin. Chem. Biol.* **21**, 144–153 (2014).
35. Maeda, K., Poletto, M., Chiapparino, A. & Gavin, A. C. A generic protocol for the purification and characterization of water-soluble complexes of affinity-tagged proteins and lipids. *Nat. Protoc.* **9**, 2256–2266 (2014).
36. Geijtenbeek, T. B., Westerman, J., Heerma, W. & Wirtz, K. W. Phosphatidylcholine transfer protein from bovine liver contains highly unsaturated phosphatidylcholine species. *FEBS Lett.* **391**, 333–335 (1996).
37. Iglesias-Artola, J. M. *et al.* Quantitative imaging of lipid transport in mammalian cells. *Nature* **646**, 474–482 (2025).
38. Kirschbaum, C. *et al.* Following phospholipid transfer through the OmpF(3)-MlaA-MlaC lipid shuttle with native mass spectrometry. *Proc. Natl. Acad. Sci. U. S. A.* **122**, e2420041122 (2025).
39. Symons, J. L. *et al.* Lipidomic atlas of mammalian cell membranes reveals hierarchical variation induced by culture conditions, subcellular membranes, and cell lineages. *Soft Matter* **17**, 288–297 (2021).
40. Morita, S. Y. & Ikeda, Y. Regulation of membrane phospholipid biosynthesis in mammalian cells. *Biochem. Pharmacol.* **206**, 115296 (2022).
41. Kapushesky, M. *et al.* Gene expression atlas at the European bioinformatics institute. *Nucleic Acids Res.* **38**, D690–698 (2010).
42. Gorden, D. L. *et al.* Biomarkers of NAFLD progression: a lipidomics approach to an epidemic. *J. Lipid Res.* **56**, 722–736 (2015).

43. Fahy, E. Biomarkers of NAFLD progression: a lipidomics approach to an epidemic. Part 1: Liver (2018). Metabolomics Workbench. Study ID: ST000915. Project DOI: https://doi.org/10.21228/M8V961
44. Koay, Y. C. Metabolomics studies on human cardiac samples (2023). Metabolomics Workbench. Study ID: ST003104. Project DOI: https://doi.org/10.21228/M8N42X
45. Hunter, B. Lipidomics analysis within healthy donors and end-stage heart failure with a focus on ischaemic cardiomyopathy with diabetes (2024). Metabolomics Workbench. Study ID: ST003275. Project DOI: https://doi.org/10.21228/M83529
46. Passaro, S. *et al.* Boltz-2: Towards Accurate and Efficient Binding Affinity Prediction. *bioRxiv*, 2025.2006.2014.659707 (2025).
47. Bennett, J. L. *et al.* Uncovering hidden protein modifications with native top-down mass spectrometry. *Nat. Methods* **22**, 2127–2137 (2025).
48. Abramson, J. *et al.* Accurate structure prediction of biomolecular interactions with AlphaFold 3. *Nature* **630**, 493–500 (2024).
49. Horibata, Y. *et al.* StarD7 Protein Deficiency Adversely Affects the Phosphatidylcholine Composition, Respiratory Activity, and Cristae Structure of Mitochondria. *J. Biol. Chem.* **291**, 24880–24891 (2016).
50. Elegheert, J. *et al.* Lentiviral transduction of mammalian cells for fast, scalable and high-level production of soluble and membrane proteins. *Nat. Protoc.* **13**, 2991–3017 (2018).
51. Bligh, E. G. & Dyer, W. J. A rapid method of total lipid extraction and purification. *Can. J. Biochem. Physiol.* **37**, 911–917 (1959).
52. Yu, F. *et al.* Analysis of DIA proteomics data using MSFragger-DIA and FragPipe computational platform. *Nat Commun* **14**, 4154 (2023).
53. Demichev, V. *et al.* dia-PASEF data analysis using FragPipe and DIA-NN for deep proteomics of low sample amounts. *Nat Commun* **13**, 3944 (2022).
54. Perez-Riverol, Y. *et al.* The PRIDE database at 20 years: 2025 update. *Nucleic Acids Res.* **53**, D543–D553 (2025).
55. Kong, A. T., Leprevost, F. V., Avtonomov, D. M., Mellacheruvu, D. & Nesvizhskii, A. I. MSFragger: ultrafast and comprehensive peptide identification in mass spectrometry-based proteomics. *Nat. Methods* **14**, 513–520 (2017).
56. Pettersen, E. F. *et al.* UCSF Chimera-a visualization system for exploratory research and analysis. *J. Comput. Chem.* **25**, 1605–1612 (2004).
57. Huang, J. *et al.* CHARMM36m: an improved force field for folded and intrinsically disordered proteins. *Nat. Methods* **14**, 71–73 (2017).
58. Van Der Spoel, D. *et al.* GROMACS: fast, flexible, and free. *J. Comput. Chem.* **26**, 1701–1718 (2005).
59. Jo, S., Kim, T., Iyer, V. G. & Im, W. CHARMM-GUI: a web-based graphical user interface for CHARMM. *J. Comput. Chem.* **29**, 1859–1865 (2008).

60. Bussi, G., Donadio, D. & Parrinello, M. Canonical sampling through velocity rescaling. *J. Chem. Phys.* **126**, 014101 (2007).
61. Bernetti, M. & Bussi, G. Pressure control using stochastic cell rescaling. *J. Chem. Phys.* **153**, 114107 (2020).
62. Hess, B., Bekker, H., Berendsen, H. J. C. & Fraaije, J. G. E. M. LINCS: A linear constraint solver for molecular simulations. *J. Comput. Chem.* **18**, 1463–1472 (1997).
63. Hunter, J. D. Matplotlib: A 2D Graphics Environment. *Computing in Science & Engineering* **9**, 90–95 (2007).
64. Humphrey, W., Dalke, A. & Schulten, K. VMD: visual molecular dynamics. *J. Mol. Graph.* **14**, 33–38, 27–38 (1996).
65. Nichols, J. W. & Pagano, R. E. Use of resonance energy transfer to study the kinetics of amphiphile transfer between vesicles. *Biochemistry* **21**, 1720–1726 (1982).
66. Nichols, J. W. & Pagano, R. E. Resonance energy transfer assay of protein-mediated lipid transfer between vesicles. *J. Biol. Chem.* **258**, 5368–5371 (1983).

Figures

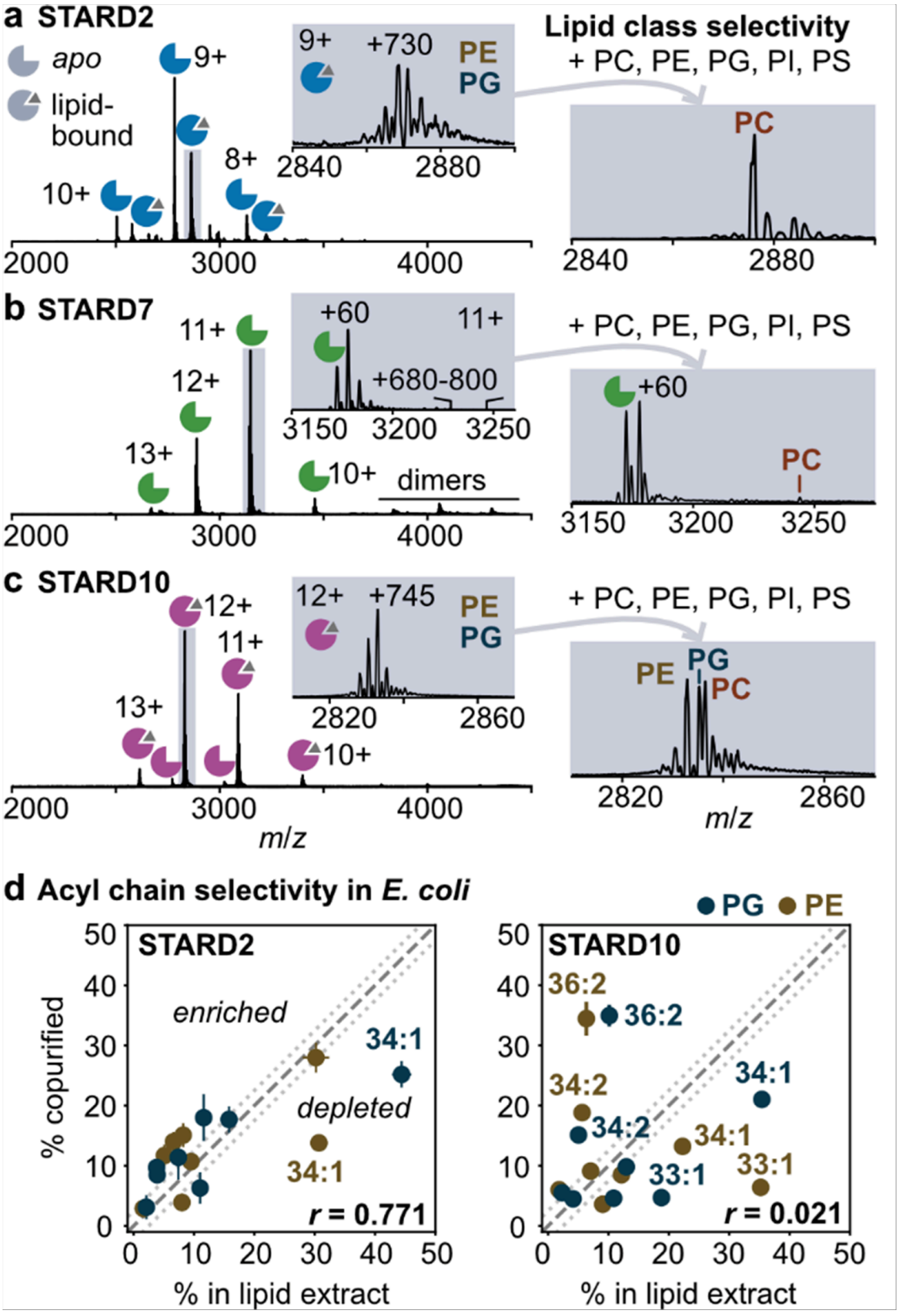


Figure 1

Phospholipid binding preferences of StARD proteins *in vitro*. (**a-c**) Native mass spectra of STARD2, STARD7 and STARD10 expressed in *E. coli*. Peaks assigned as bacterial PE and PG binding are observed in the mass spectra of STARD2 (**a**) and STARD10 (**c**). The native mass spectrum of STARD7 (**b**) shows that it is purified in its *apo* form and binds acetate (+60 Da). When incubated with an equimolar mixture of DOPC, DOPE, DOPG, DOPI and DOPS, STARD2 and STARD7 bind exclusively to DOPC, whereas

STARD10 binds DOPC, DOPE and DOPG in similar amounts. (**d**) Correlation plots showing the abundances of lipids copurified with STARD2 and STARD10 vs. the abundances of lipids across the bacterial cell. STARD2 show a high correlation whereas STARD10 enriches di-unsaturated lipids (34:2 and 36:2) over mono-unsaturated lipids (33:1 and 34:1).

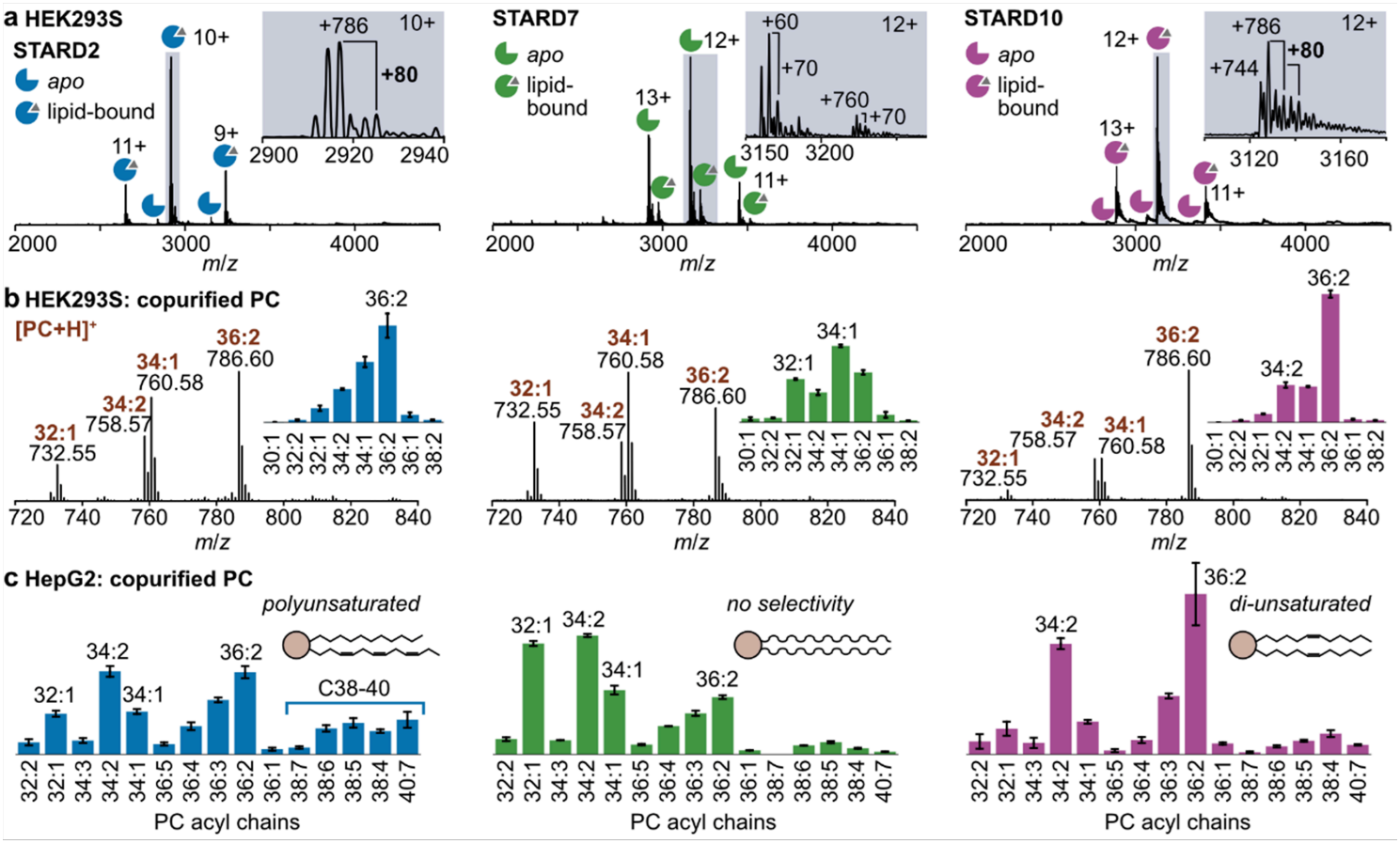


Figure 2

Endogenous lipids binding to STARD2, STARD7 and STARD10 in human cell lines. (**a**) Native mass spectra of the LTPs expressed in HEK293S cells. MS^2 spectra reveal that PC copurifies with all proteins in HEK293S (**b**) and HepG2 cells (**c**). STARD2 binds PC lipids with a preference for long unsaturated acyl chains, STARD7 copurifies with PC without apparent acyl chain selectivity and STARD10 enriches di-unsaturated PC. STARD10 also copurifies with PE(-P) and PG (only visible in negative ion mode).

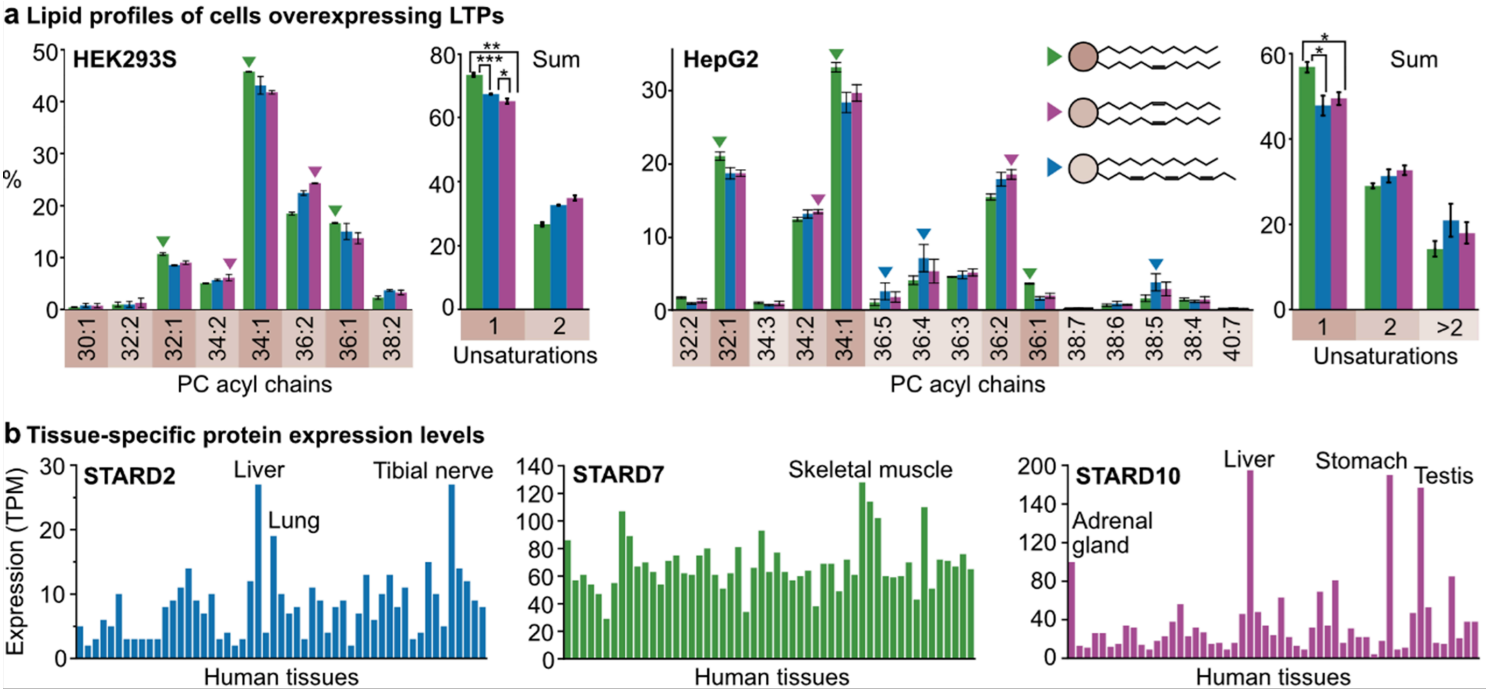


Figure 3

Expression levels of StARD proteins and feedback on lipid metabolism. (**a**) Relative quantification of PC lipids in cells overexpressing STARD2, STARD7 or STARD10 for 48 h. Overexpression of these LTPs changes the PC acyl chain profiles in HEK293S and HepG2 cells. (**b**) Expression levels of STARD2, STARD7 and STARD10 in human tissues. Data were downloaded from the Gene Expression Atlas (http://www.ebi.ac.uk/gxa).[41] For full description of tissues refer to Figure S20.

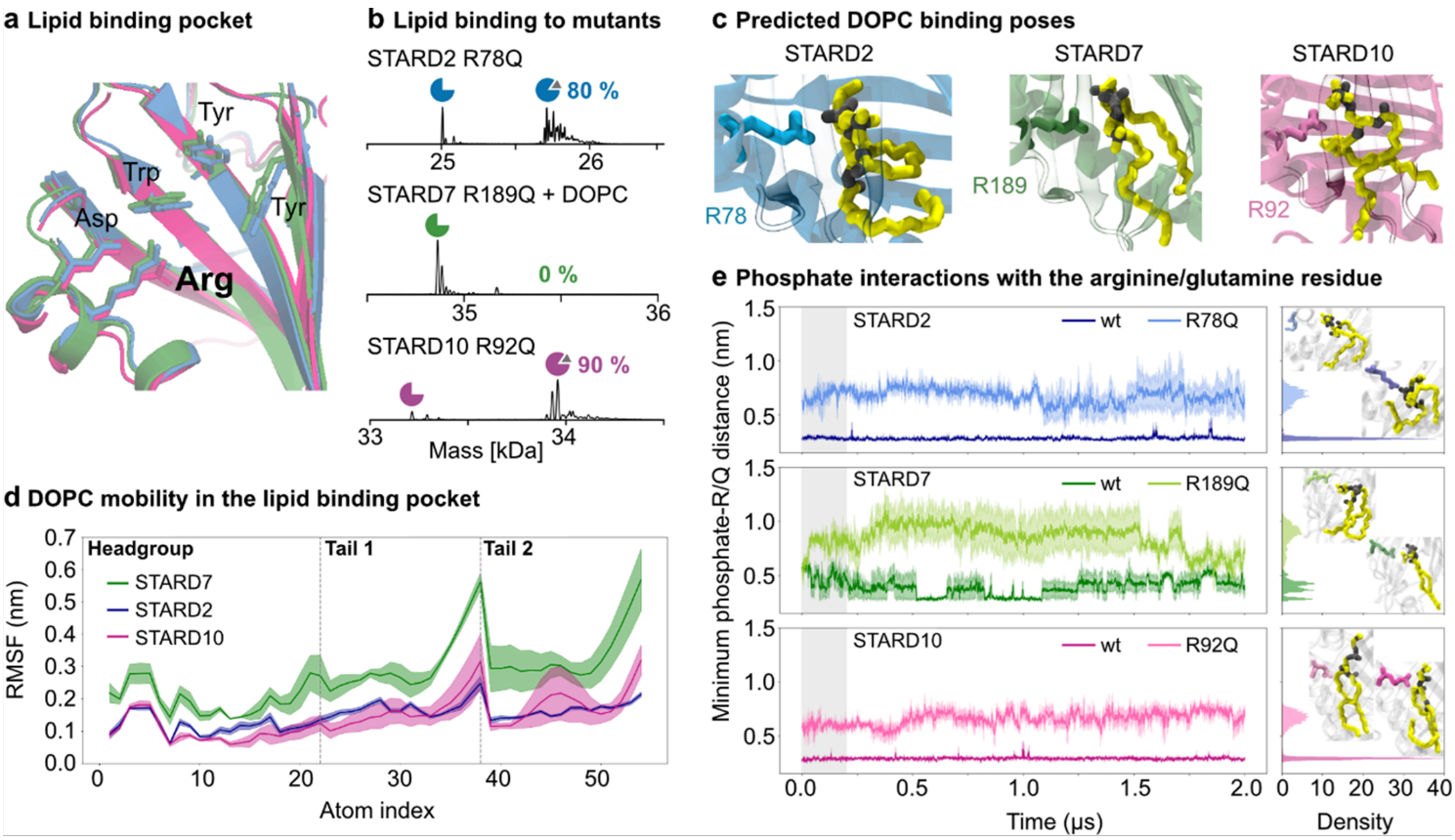


Figure 4

Role of a conserved arginine for phospholipid binding in STARD2, STARD7 and STARD10. **a.** Overlay of lipid binding pockets, with the aromatic cage and Asp-Arg residues highlighted (AlphaFold structures). **b.** Quantification of lipid binding to R→Q mutants based on deconvolved native mass spectra. Mutation of the conserved arginine leads to loss of lipid binding in STARD7 but not in STARD2 or STARD10 (lipids are copurified upon expression in *E. coli*). **c.**Boltz-2 predicted structures of DOPC-bound STARD2, STARD7 and STARD10. **d.** Mobility of DOPC inside the cavity as shown by the RMSF of DOPC in AA-MD. The shaded region is the standard error of mean. **e.** Minimum distance between the phosphate group of DOPC and the conserved arginine (dark traces) or the mutated glutamine (light traces) residues. Insets show the lipids inside the binding pockets at the end of the simulation (R in dark, Q in light). The shaded region around the solid line is the standard error of mean. The first 0.2 μs of simulation, shaded in grey, were excluded in the probability density calculation and the RMSF calculation.

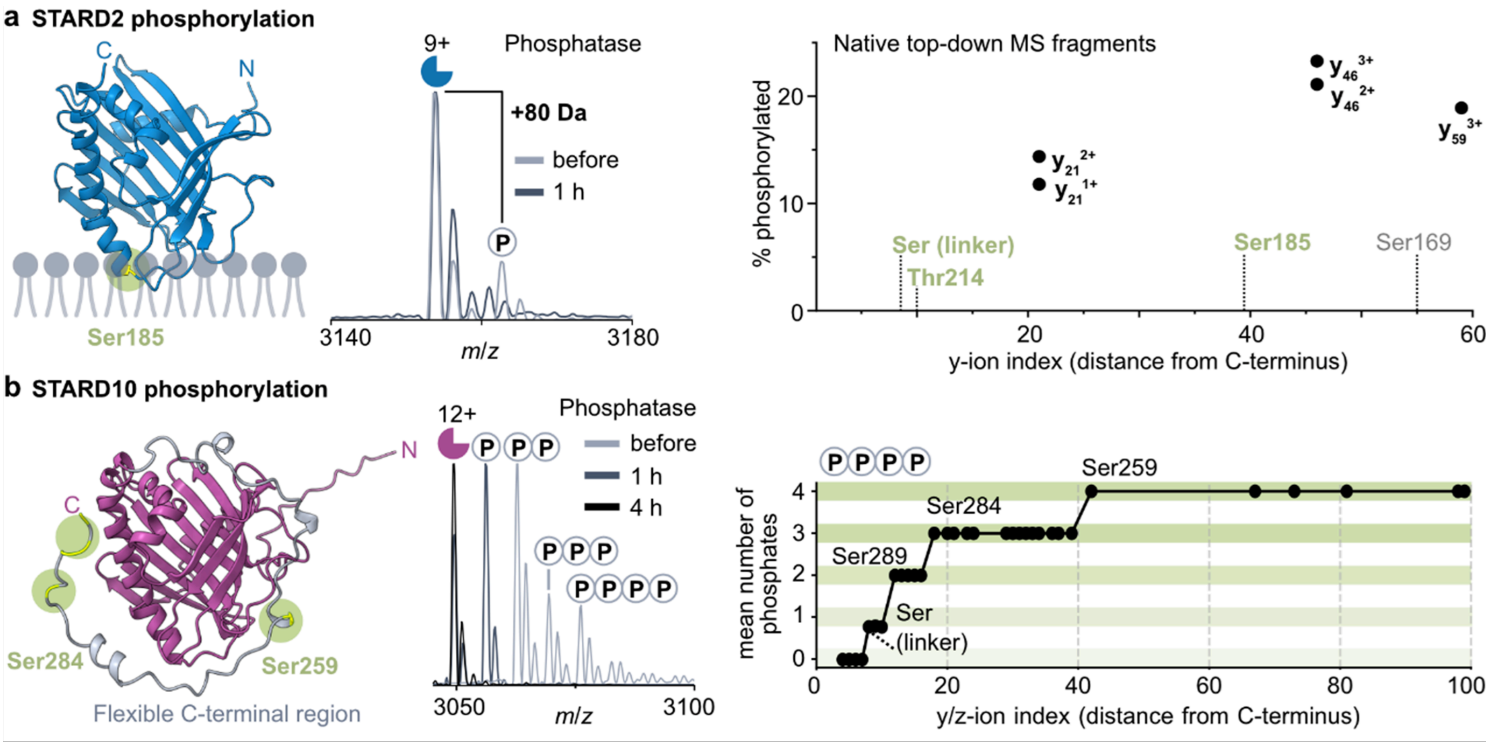


Figure 5

Phosphorylation of STARD2 and STARD10 in membrane-interacting regions. (**a**) Native MS before and after treatment with λ-phosphatase shows that STARD2 is partially phosphorylated (ca. 10 %). Analysis of phosphorylated C-terminal protein fragments generated by native top-down MS localizes phosphorylation at the C-terminus and at Ser185. (**b**) Treatment of STARD10 with λ-phosphatase shows that STARD10 is phosphorylated at up to four sites. The sites were mapped to two constitutive phosphorylation sites (Ser259 and Ser284) and up to two partially occupied sites in the C-terminus based on native top-down MS. Structures were generated using Alphafold3.[48]

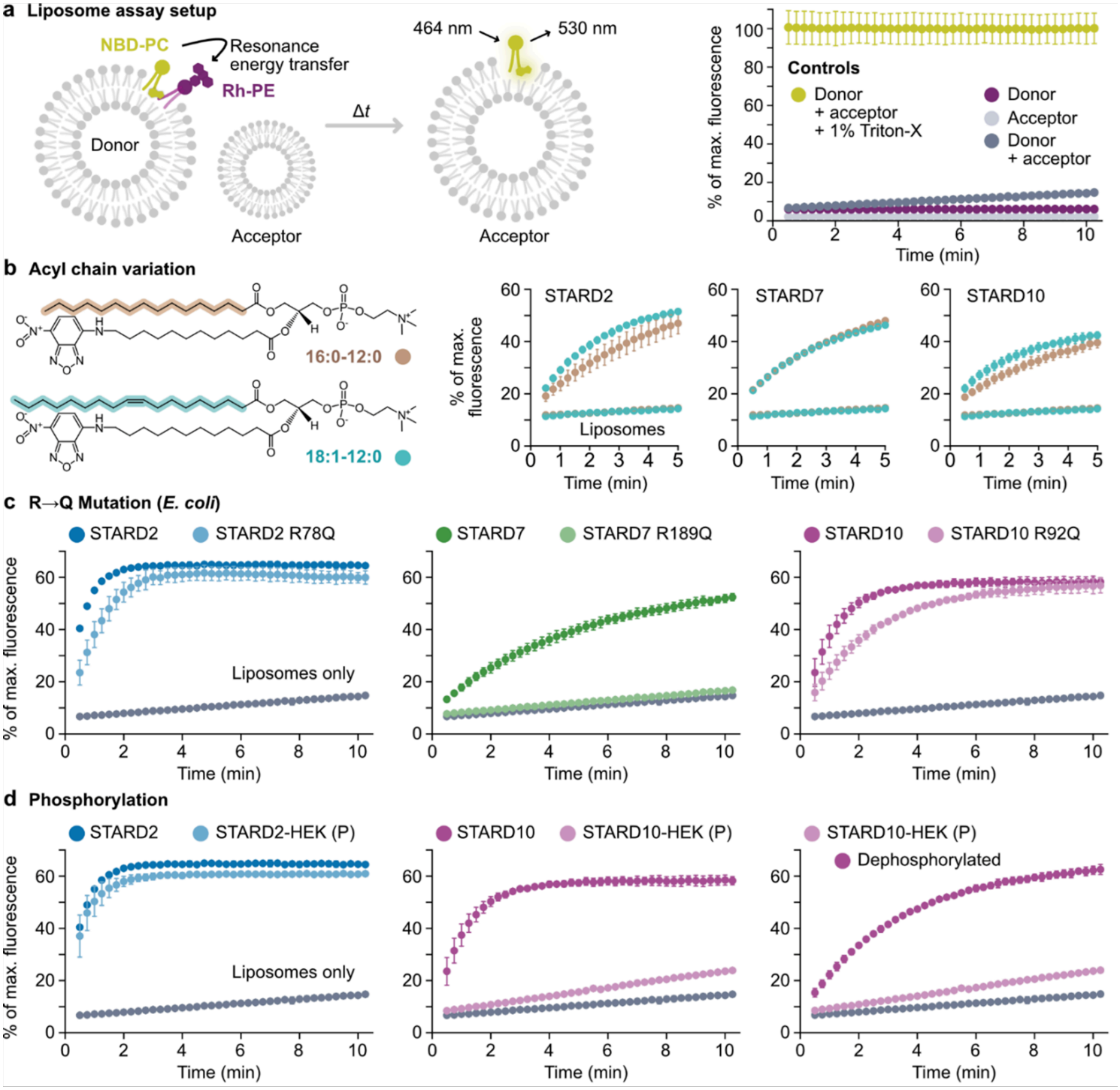


Figure 6

Liposome assays correlating acyl chain selectivities, binding pocket mutation and phosphorylation with lipid transfer activity *in vitro*. (**a**) The fluorescence of NBD-PC is quenched by Rh-PE in donor liposomes and increases as NBD-PC is transported to acceptor liposomes. Control measurements were performed for individual liposomes, mixed liposomes and mixed liposomes treated with Triton-X to determine the maximum fluorescence. (**b**) STARD2 and STARD10 transport unsaturated NBD-PC faster than saturated NBD-PC, whereas STARD7-mediated lipid transfer is not affected by acyl chains. (**c**) Arginine-to-glutamine mutation abolishes PC transfer in STARD7 but not in STARD2 and STARD10. (**d**)

Phosphorylation (P) of STARD10 abolishes its lipid transfer activity, which can be recovered by dephosphorylation.

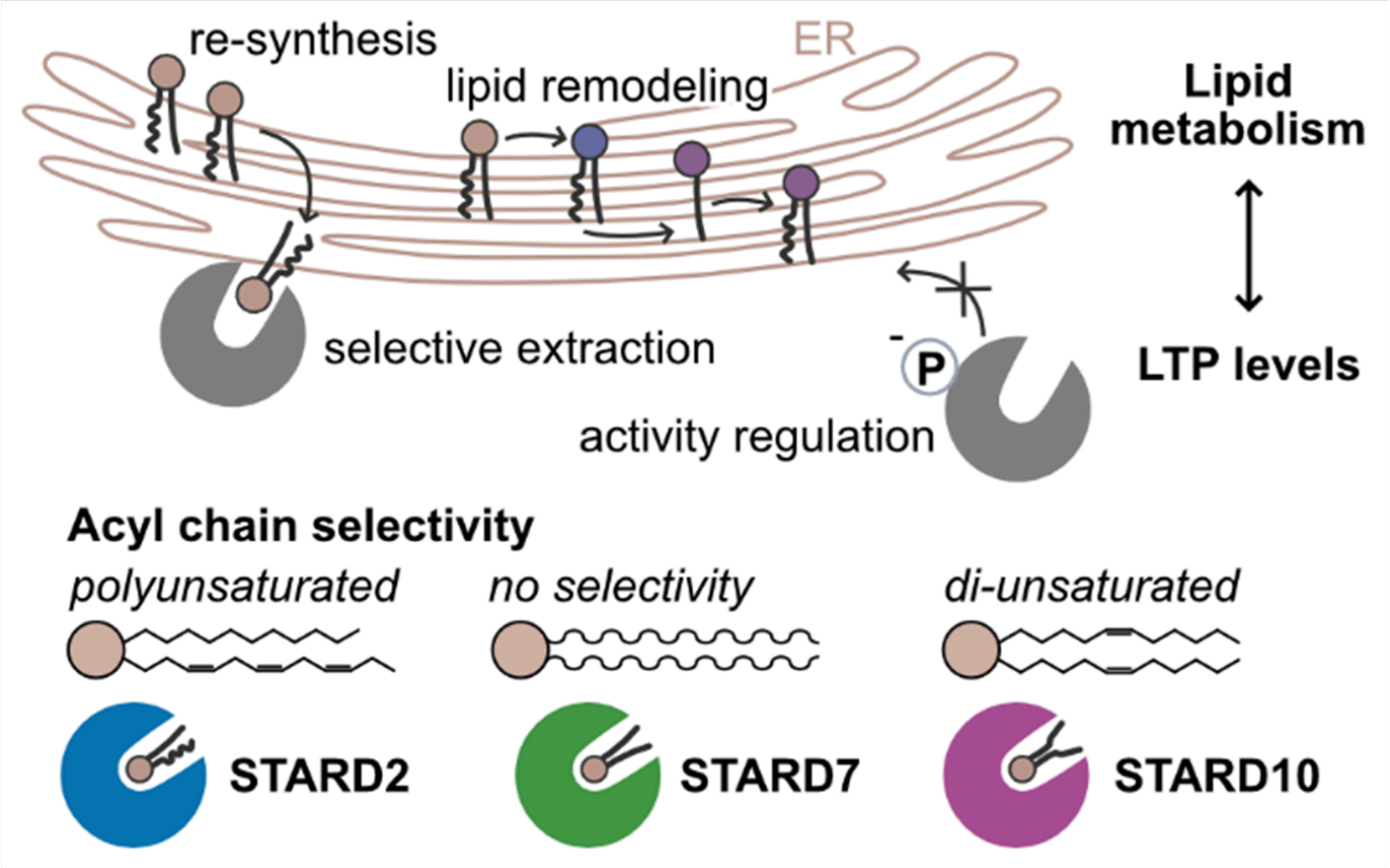


Figure 7

Proposed mechanism for the interplay between LTP-mediated lipid transfer and cellular lipid metabolism. Acyl chain-selective extraction of PC from the ER could lead to replenishment of the depleted acyl chain pool, causing an overall increase in the abundance of the extracted PC. The acyl chain distributions of other phospholipids are also affected via acyl chain remodeling. Phosphorylation could serve as a regulatory mechanism to inhibit protein–membrane association and reduce lipid transfer activity.

Supplementary Files

This is a list of supplementary files associated with this preprint. Click to download.

- Rawfiles.pdf
- 260113SupportingInformation.pdf